ELSEVIER

Journal of Chromatography A, 746 (1996) 137–145

JOURNAL OF CHROMATOGRAPHY A

High-speed particle separation and steric inversion in thin flow field-flow fractionation channels

Keith D. Jensen[1], S. Kim R. Williams, J. Calvin Giddings*

Field-Flow Fractionation Research Center, Department of Chemistry, University of Utah, Salt Lake City, UT 84112, USA

Received 11 December 1995; revised 28 March 1996; accepted 28 March 1996

Abstract

The performance of thin (down to 71 μm thick) flow field-flow fractionation (flow FFF) channels was examined at both high channel flow-rates (up to ~47 ml/min) and cross flow-rates (up to ~11 ml/min). High levels of retention were observed, suggestive of good performance characteristics. Supporting this expectation, four sizes (0.04–0.30 μm) of polystyrene latex microbeads were baseline separated in under 3 min. Nonetheless, a plate height analysis showed that performance was still less than theoretically expected.

Fast steric-hyperlayer separations of larger latex beads were observed in the same systems. Furthermore, it was shown that the steric inversion diameter was shifted down to ~0.23 μm, thus expanding the size range to which this FFF mode is applicable. The steric inversion phenomenon observed using narrow latex standards was shown to be consistent with that found for a polydisperse polyvinylchloride latex.

Keywords: Field-flow fractionation; Polystyrene latex microbeads; Steric inversion; Polyvinylchloride

1. Introduction

Field-flow fractionation (FFF) is a family of separation and characterization techniques that has been applied to many different macromolecular and particulate samples [1,2]. Separation takes place in a channel that is constructed by removing a rectangular section with triangular ends from a thin plastic spacer. The spacer is clamped between two walls and a stream of carrier liquid is introduced to transport sample components down the length of the channel. Flow is characterized by a parabolic profile established across the thickness w of the channel (see Fig. 1a). The flow velocity is fastest at the center of the channel and decreases to zero at the walls because of frictional drag. A field is applied in a direction perpendicular to the flow axis to drive the component particles (or polymers) towards one wall (the accumulation wall). This field-induced migration is counteracted by the opposing transport of particles due to their diffusion away from the wall. At equilibrium, exponential concentration distributions of different mean layer thicknesses (e.g., l_1, l_2,...) are established at the accumulation wall for each different component [3]. Smaller particles, which have larger diffusion coefficients, will generally have larger mean layer thicknesses and will be transported by faster flowing streamlines of the parabolic flow than their larger counterparts (see Fig. 1a). Thus,

*Corresponding author.

[1]Present address: Department of Pharmaceutics and Pharmaceutical Chemistry, University of Utah, Salt Lake City, UT 84112, USA.

0021-9673/96/$15.00
PII S0021-9673(96)00288-9

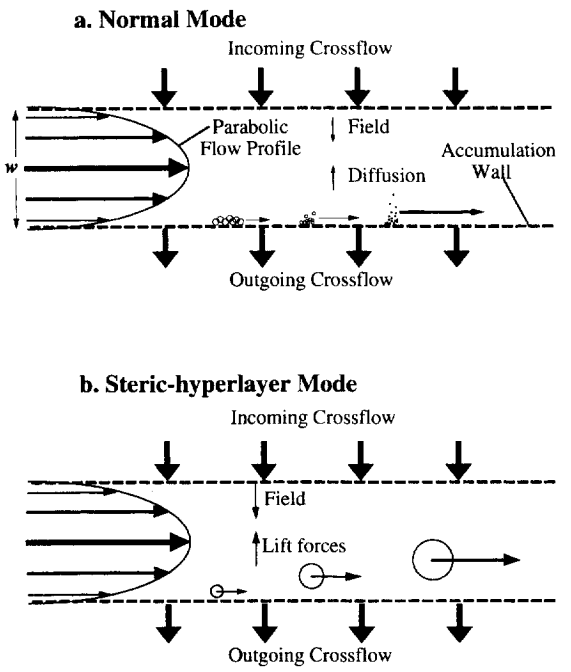

Fig. 1. Separation mechanisms of (a) normal mode in which smaller particles elute first because they diffuse further from the accumulation wall and are transported by faster streamlines than large particles and (b) steric-hyperlayer mode in which hydrodynamic lift forces propel large particles further away from the wall than small particles, leading to the elution of large particles first and small particles last.

small particles elute before large particles. This elution sequence, characterizing the normal mode of FFF operation, is found for most macromolecules and submicron particles.

Any 'field' that induces migration of the sample to the accumulation wall can be used. The most common FFF fields include crossflow, sedimentation, thermal gradient, and electrical [1,2]. The work reported in this paper was done using a crossflow of liquid as the field and is termed flow FFF.

According to the Stokes–Einstein equation [4], the diffusion coefficient is inversely proportional to particle diameter d. For diameters larger than approximately 1 μm, diffusion is insignificant and another mode of separation prevails. In this steric-hyperlayer mode, particles experience steric effects and hydrodynamic lift forces which drive them away from the wall [5–7]. For each particle size, an equilibrium position is established at the point where the force of the applied field is equal to the opposing lift forces. Because larger particles experience larger lift forces, the larger particles form equilibrium bands further from the accumulation wall and are transported more rapidly down the channel than smaller particles (see Fig. 1b) [5–7]. The elution order is opposite to that of the normal mode.

The steric inversion diameter d_i, which signifies the point of transition between the normal and the steric-hyperlayer modes, has been reported to occur between 0.3–3 μm [8–10]. A sample with a broad size distribution that spans across the steric inversion diameter (e.g., 0.2–10 μm) will experience coelution of two components of different d values at any one time, the smaller component eluting in the normal mode and the larger in the steric-hyperlayer mode. The steric inversion diameter is dependent on experimental parameters with d_i generally expected to decrease with increasing field strength and channel flow velocity (or shear rate) [8]. One objective of this work has been to find out if d_i can be reduced below typical values (0.5–1.0 μm) found for flow FFF by such means. Shifting d_i to either smaller or larger values may allow separation of the entire sample size range in only one mode.

A second objective of this study is to determine if separative performance in flow FFF can be enhanced by using high field strengths and shear rates. Because shear rate increases inversely with the square of channel thickness at constant flow-rate, thin channels are essential for such an investigation.

2. Theory

The retention ratio R is the ratio of the void time (time required for the channel flow to sweep out one channel volume) to the retention time (time required for the sample component to elute). The retention ratio can also be written as [10]

$$R = 6\lambda + 3\frac{\gamma d}{w} \quad (1)$$

where λ is the retention parameter (equal to l divided by the channel thickness w) and γ is the dimensionless steric correction factor (generally of order unity and assumed to equal unity in this work). For very small particles, the second term on the right in Eq. (1) becomes negligible because d/w is small in

comparison to l/w (or λ), which is large as a result of the fast diffusion of small particles. As a result, R in the normal mode is often approximated as 6λ. Thus, for normal mode flow FFF, R becomes [11]

$$R \cong 6\lambda = \frac{6DbL}{w\dot{V}_c} \quad (2)$$

where D is the diffusion coefficient, b is the channel breadth, L is the volume-based channel length, and $\dot{V}_c$ is the cross flow-rate. This approximation overestimates R by 1.0% for $R=0.03$ and by 5.6% for $R=0.15$.

For very large particles, d/w is significant and the slow diffusion causes l/w to be small. Consequently, R in the steric-hyperlayer mode approaches $3\gamma d/w$. Eq. (1) is used for particles of intermediate size where both mechanisms have a significant role in retention.

For simplicity, the γ factor is usually set as unity. However, experimentally derived γ values have been shown to be both greater than and less than unity (γ must be greater than zero for any observed peak) [12,13]. Values of $\gamma>1$ are caused by hydrodynamic lift forces that drive particles away from the wall [5,7]. The magnitude of these lift forces increases with increasing channel flow velocities. Values of $\gamma<1$ are caused by retardation effects that decrease the particle's velocity relative to the surrounding fluid as the particle is forced close to the accumulation wall [14]. Retardation effects become more pronounced when low channel flow velocities and high field strengths are used. Consequently, the value for γ varies as a function of experimental conditions and the interplay between hydrodynamic lift forces and retardation effects on particles.

Band broadening in FFF systems can be measured by the plate height H, comprised of the following components [3,15]

$$H = H_D + H_n + H_p + \Sigma H_i \quad (3)$$

where H_D is the longitudinal diffusion contribution, H_n is due to nonequilibrium band broadening, H_p is the sample polydispersity contribution, and ΣH_i is the sum of contributions due to system nonidealities. The H_D term is usually negligible in FFF because of slow sample diffusion [15]. The ΣH_i term is negligible for analyses in ideal FFF systems but may make a significant contribution to H in some real systems. The main contributors to plate height considered here are H_p and H_n. For perspective, it should be kept in mind that H_p is not a true band broadening term but is a separation term in which a polydisperse sample is fractionated into differently positioned components, giving an apparent band broadening effect as a result of separation.

Since the latex particles used in this work possess a finite size distribution, there is a significant polydispersity contribution to the plate height which can be calculated as [15]

$$H_p = LS_d^2\left(\frac{\sigma_d}{d}\right)^2 \quad (4)$$

where S_d is the diameter based selectivity (equal to unity for flow FFF) and σ_d is the standard deviation in the particle diameter of the sample.

Nonequilibrium band broadening occurs when particles of a given size diffuse into different flow velocity streamlines and are momentarily transported faster or slower than the average speed. The magnitude of H_n is dependent on λ, w, d, and the mean channel flow velocity $\langle v\rangle$ as shown by the following equation derived from reference [16]

$$H_n = \frac{24\lambda^4(1-10\lambda+28\lambda^2)}{(d/2w)+\lambda(1-2\lambda)}\frac{w^2\langle v\rangle}{D} \quad (5)$$

The above equation, which corrects for steric effects and applies when $R\leq 0.5$ and $d\ll w$, predicts that H_n will increase linearly with increasing flow velocity. To reduce H_n, most of the early work in normal mode flow FFF utilized low channel flow-rates (<1.8 ml/min). For example, the first separation of polystyrene latex beads was obtained using a channel flow-rate $\dot{V}$ of 0.1 ml/min and a cross flow-rate $\dot{V}_c$ of 0.21 ml/min [17]. Separation of the latex beads ranging in size from 0.091 μm to 0.481 μm took 7 h and produced poorly resolved peaks. In 1986, Wahlund et. al. [11] showed that the separation of a mixture of M_r 35 000–750 000 sulfonated polystyrene could be achieved in less than 40 min when a high channel flow-rate of 7.2 ml/min was used. More recently, Botana et al. [18] reported separations of submicron polystyrene latex particles using channel flow-rates of 8 ml/min.

In this paper, we show that high flow-rates can be used effectively despite the linear dependence of H_n

on $\langle v \rangle$. This dependence is offset by using flow-rates (which, as shown by Eq. (2), reduce λ) and thin channels (which will be discussed later in this paper).

3. Experimental

The flow FFF channel system was assembled by sandwiching a Mylar spacer with the channel form cut out and a semipermeable membrane (YM10, Amicon, Danvers, MA, USA) between two Plexiglas blocks with inset ceramic frit panels [19]. The frits allow free passage of the crossflow liquid across the channel. Sample is prevented from flushing out through a frit by the membrane that is layered over the frit to form the accumulation wall. A variety of different channels was assembled using Mylar spacers of different thicknesses. All of the channels had dimensions of 38.4 cm tip-to-tip length, 2.0 cm breadth, and thicknesses ranging between 71 and 179 μm.

The channel breadth and length are determined by the dimensions of the Mylar spacer. However, the channel thickness w is not necessarily equal to the spacer thickness because of the compressibility of the membrane [19,20]. Different channel thicknesses can result upon reassembly of the channel with a different strip of membrane. Consequently, the w values for each channel were calculated from the sterically corrected retention times [16] of particle standards of known diameters. The values reported in this work are an average of determinations using 3 to 4 different standards.

Two different channel and crossflow pump combinations were used depending on whether the desired flow-rates were below or above 10 ml/min. In the former case, the channel and cross flows were controlled by a Spectra-Physics Isochrom LC pump (San Jose, CA, USA) and a syringe pump (built in-house), respectively. In the latter case, an FMI QD pump (Oyster Bay, NY, USA) was used to control $\dot{V}$, a Spectra-Physics Isochrom LC pump was used for $\dot{V}_c$, and a syringe pump was used to sweep the sample plug into the channel at a low flow-rate (e.g. 1 ml/min). A variable pressure regulator (Optimize Technologies, Bend, OR, USA) was used to ensure that the incoming and outgoing $\dot{V}$ (and consequently the $\dot{V}_c$) were equal by providing additional back pressure as needed on the $\dot{V}$ or $\dot{V}_c$ outlet. Precise volumes were injected using an injection valve with a 20 μl sample loop (Valco Instruments, Houston, TX, USA). Detection of eluting particles was accomplished with a Linear UV-106 detector (Thermo Separation Products, Fremont, CA, USA) set at 254 nm. Data were recorded using a Quantigraph chart recorder (Houston Instruments, Austin, TX, USA) and an IBM-PC compatible computer.

The stopflow method of injection [21], which was used in this work, involves transport of the sample into the channel, diverting the channel flow to allow the sample components to relax to their respective equilibrium positions in the presence of only the crossflow, and then resuming the channel flow for the separation and elution stage. Reproducible placement of the sample plug on the accumulation wall for stopflow relaxation is essential for reproducible results. In experiments involving high $\dot{V}$, manually diverting the channel flow at precisely the desired time becomes difficult. For $\dot{V} > 10$ ml/min, a computer-controlled Rheodyne 7163 pneumatic valve (Cotati, CA, USA) was used to reproducibly implement stopflow and start a run. Another alternative used in this work involved sample introduction using a low $\dot{V}$, sample relaxation with no channel flow, and separation using a high $\dot{V}$. This setup employs a four-way valve to connect either the high or low flow-rate pump to the FFF system. The use of one pump for both sample introduction and separation was impractical because of the short stopflow times (4 s for $\dot{V}_c = 10.7$ ml/min and a 0.63 ml channel volume).

The carrier was doubly distilled water containing 0.1% by volume of the surfactant FL-70 (Fisher Scientific, Fair Lawn, NJ, USA) and 0.02% (w/w) sodium azide. All particle standards were obtained from Duke Scientific (Palo Alto, CA, USA) and Seradyn, (Indianapolis, IN, USA). These consisted of polystyrene (PS) latex microbeads with nominal diameters and standard deviations in the diameters of 0.040 μm$\pm$0.0018 μm, 0.091$\pm$0.0058, 0.135$\pm$0.0057, and 0.300$\pm$0.003; additional microbeads used in the steric inversion work had nominal diameters of 0.054 μm, 0.107, 0.220, 0.232, 0.330, 0.398, 0.426, 0.496, 0.596, 0.652, 0.742, 0.806, 0.845, 0.868, 0.913, 0.993, 1.335, 1.635, 2.010, and 2.062 μm. The polyvinylchloride (PVC)

latex was obtained from an industrial source and had a diameter range of 0.2 μm to 2 μm.

An S-450 scanning electron microscope (Hitachi Scientific Instruments, Tokyo, Japan) was used to examine fractions collected at the detector outlet. The fractions were deposited on a 13 mm Nuclepore membrane filter (0.1 μm pores) which was then mounted on an aluminum stub. The particles were coated with a thin layer of gold and palladium. Typical magnifications were 6000× with an acceleration voltage of 20 kV.

4. Results and discussion

A normal mode flow FFF separation of four latex bead sizes achieved in an 85 μm thick channel is shown in Fig. 2. The latex beads were separated with near baseline resolution in less than 3 min. The channel flow-rate of 29.9 ml/min (or $\langle v \rangle = 29$ cm/s) is among the highest used to date for normal mode separations. Because of the thin channel, the shear rate at the wall, $6\langle v \rangle/w$, was extraordinarily high, 2.0×10^4 s^{-1}. A correspondingly high $\dot{V}_c$ of 10.7 ml/min was required to resolve the peaks from the system transient.

In previous works, the use of high $\dot{V}_c$ has resulted in reversible immobilization of sample on the membrane [6,11]. Consequently, it has not been possible to work at the low λ and retention ratio levels required for optimum efficiency (see Eq. (5)). However, the latex beads shown in Fig. 2 are highly retained with R values ranging from 0.031 to 0.0076 (corresponding to retention volumes of 33 to 132 channel volumes). The mechanism at play in making possible this unusually high speed separation at high $\dot{V}$ and $\dot{V}_c$ is not fully understood and warrants more in-depth study. In particular, the role of the high shear rate in preventing reversible immobilization (a poorly understood phenomenon) should be investigated. There is little doubt that the key structural feature giving rise to such extreme operating conditions as used here is the thinness of the channel. The small w leads to high shear rates which appears to make operation at smaller λ values possible. The cross flow-rate $\dot{V}_c$ must be increased in inverse proportion to w (see Eq. (2)) just to keep λ constant; it must increase further if λ is to be reduced in an attempt to reach higher efficiencies (see Eq. (5)). With a small λ and w both reducing H, the channel flow-rate $\dot{V}$ can be substantially increased in a quest for higher speed.

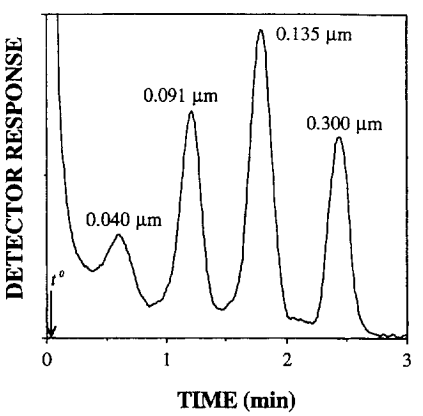

Fig. 2. Fractogram showing normal mode separation of PS latexes of indicated diameters at high flow-rates. The channel thickness $w = 85$ μm and the flow-rates are $\dot{V} = 29.9$ ml/min and $\dot{V}_c = 10.7$ ml/min. Void time t^0 is shown.

It should be noted that the cross flow-rate used here, although high, is well below the critical value of 310 ml/min (calculated for this channel) where perturbation of the parabolic flow profile by the crossflow would cause 1% error in the retention ratio [22].

The various experimental and theoretical plate heights pertaining to Fig. 2 are summarized in Table 1. The plate height obtained by direct measurement of the peak width for each particle size standard is tabulated as $H_{(obs)}$. The minimum $H_{(obs)}$ value found in previous normal mode flow FFF work with protein standards (assumed to be monodisperse) has been in

Table 1
Experimental and theoretical plate heights for the peaks shown in Fig. 2.

d (μm)	$H_{(obs)}$ (mm)	H_p (mm)	$H^a_{n(theor)}$ (mm)	$H^b_{(exp)}$ (mm)	N	N/t^c (s^{-1})
0.040	14.4	0.73	0.64	13.7	26	0.73
0.091	1.70	1.46	0.11	0.24	1500	21
0.135	0.88	0.64	0.015	0.24	1500	15
0.300	0.46	0.036	0.0038	0.42	860	5.9

[a] $H_{n(theor)}$ calculated using experimental λ and Eq. (5).
[b] $H_{(exp)} = H_{(obs)} - H_p$.
[c] $N/t = L/[H_{(exp)} \times t]$.

the range of 2 mm [23]. For the asymmetric flow FFF variant, an $H_{(obs)}$ value as low as 0.1 mm has been reported for virus particles, which can be considered to be a monodisperse sample [24]. The polydispersity corrected value $H_{(exp)}$ of 0.24 mm obtained in this work (which should be the same as $H_{(obs)}$ for a monodisperse sample) is quite remarkable considering the high flow velocity. (The $H_{(obs)}$ for the 0.040 μm latex is relatively large and may be due in part to measurement errors introduced by the incomplete separation of the peak from the system transient.)

The polydispersity contribution H_p was calculated via Eq. (4) using the standard deviations (noted earlier) reported by the supplier. Eq. (5) was used for the calculation of theoretical H_n values, shown in Table 1 as $H_{n(theor)}$. For this purpose, values for λ were calculated from the experimentally measured retention ratios as defined in Eq. (1). The results show that quite small H_n values are theoretically possible at high flow-rates providing λ and w are small. The λ value for the 0.300 μm latex was calculated from Eq. (2) using the Stokes-Einstein equation to obtain D. (We did not use Eq. (1) because the usual assumption that $\gamma = 1$ leads to a negative λ value.)

For a meaningful comparison of the experimental H with $H_{n(theor)}$, the observed plate height must be corrected for polydispersity giving $H_{(exp)}$ in Table 1. Despite the significantly larger $H_{(exp)}$ values than $H_{n(theor)}$ for all diameters, the former are among the lowest plate height values obtained for normal mode flow FFF. The discrepancy in $H_{(exp)}$ and $H_{n(theor)}$ values obtained here are likely due to system imperfections.

The number of plates N (where $N = L/H_{(exp)}$) for each peak in Fig. 2 is tabulated in Table 1. Also the number of plates generated per unit time t was calculated and listed as N/t. Up to ~20 plates/s were generated in this work. This is the highest N/t value yet reported for flow FFF.

Unlike the normal mode, good resolution in the steric-hyperlayer mode is usually observed at high flow-rates [2,6,9]. Fig. 3 is a fractogram of a steric-hyperlayer mode separation of four different latexes separated under the same conditions as those used in Fig. 2 ($\dot{V} = 29.9$ ml/min, $\dot{V}_c = 10.7$ ml/min). The well resolved peaks were again separated in less than 3 min. Using these conditions, d_i is found to be in the vicinity of 0.30 μm. Hence, the 0.30 μm latex could be resolved in either the normal or steric-hyperlayer mode separations as shown by Fig. 2 and Fig. 3.

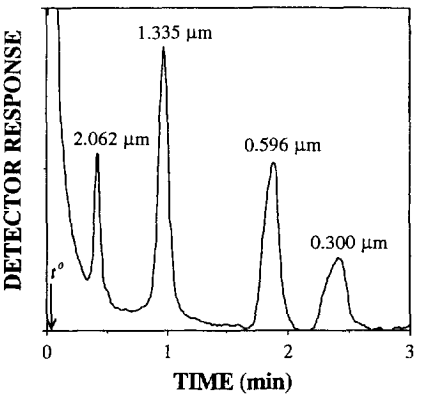

Fig. 3. Steric-hyperlayer separation of PS latex beads obtained using the same channel and flow-rates as described in Fig. 2.

As discussed in the introduction, a sample with a broad size distribution that spans the steric inversion diameter d_i will experience separation by both the normal mode mechanism (for $d < d_i$) and steric-hyperlayer mechanism (for $d > d_i$). Such a sample was used to produce Fig. 4 using a channel with $w = 75$ μm and flow-rates of $\dot{V} = 6.15$ ml/min and $\dot{V}_c = 3.02$ ml/min. This PVC latex sample has an approximate particle size range of 2 μm to 0.2 μm. Fractions were collected at the detector outlet in the time intervals indicated in Fig. 4. The scanning electron micrographs show the coelution of two distinctly different particle sizes for each fraction. The micrograph of the early eluting fraction 9 shows the presence of two discrete particle populations with a large diameter difference. This observation is much as expected since the smaller particles elute first in the normal mode and the larger particles elute first in the steric-hyperlayer mode. The difference in diameter of the two coeluting particle populations should decrease with increasing retention time; this trend is observed in the micrographs of fractions 17, 22, and 25. The series of micrographs confirm the major features expected of the steric inversion phenomenon. Similar results have been observed with sedimentation FFF [10].

The steric inversion diameter d_i is best determined by measuring R values for a series of narrow

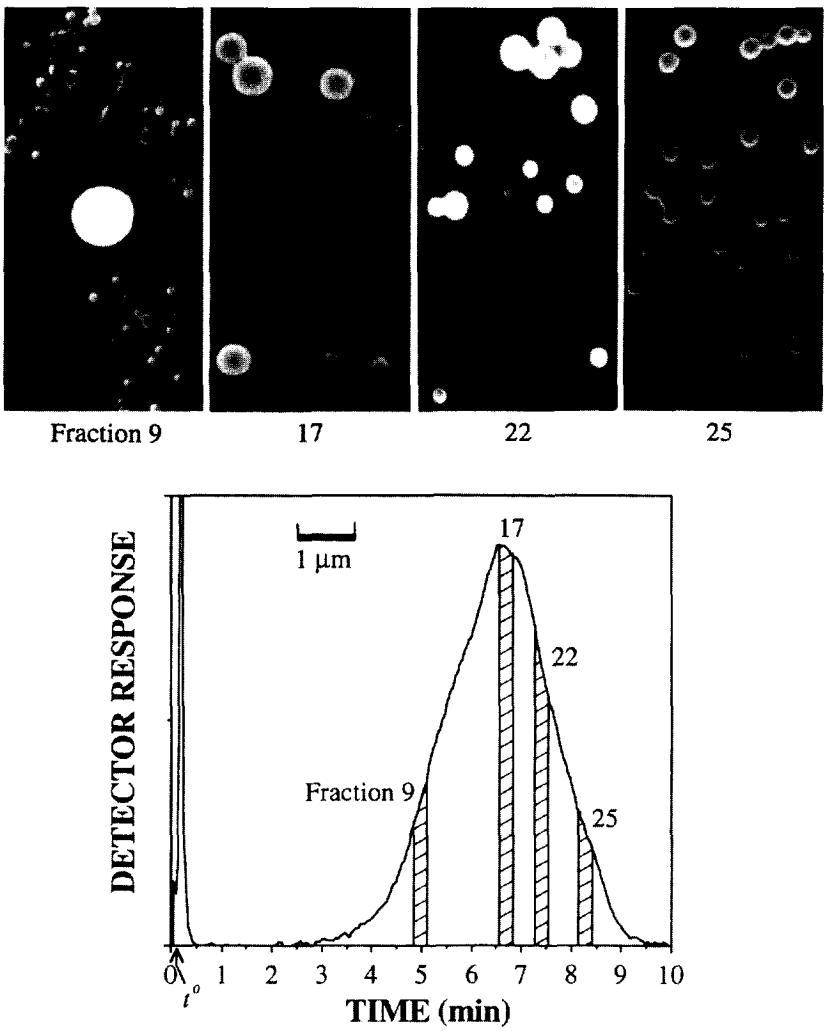

Fig. 4. Fractogram of PVC sample and scanning electron micrographs of four collected fractions showing coelution of two particle sizes at each retention time. For this run, $w=75$ μm, $\dot{V}=6.15$ ml/min, and $\dot{V}_c=3.02$ ml/min.

polystyrene latex standards. The minimum in the plot of R verses d occurs at $d=d_i$. Using this method and similar experimental conditions to that employed for the PVC sample shown in Fig. 4, the d_i was determined to be 0.40 μm.

The inversion diameter d_i can be shifted by changing experimental conditions. Fig. 5 demonstrates the changes in the relationship between the retention ratio and the particle diameter when three different channels and flow-rate conditions are employed. Using a thick (179 μm) channel and low flow-rates ($\dot{V}=3.93$ ml/min, $\dot{V}_c=0.22$ ml/min), plot a is obtained; for this plot d_i occurs at approximately 0.85 μm. When a thinner channel ($w=85$ μm) and faster flow-rates ($\dot{V}=29.9$ ml/min, $\dot{V}_c=10.7$ ml/min) are used, plot b is produced and d_i is shifted to approximately 0.30 μm. An even thinner channel ($w=75$ μm) and higher flow-rates ($\dot{V}=47.0$ ml/min, $\dot{V}_c=10.8$ ml/min) results in plot c and a d_i of 0.23 μm. The observed shifts in d_i with increasing $\dot{V}$ and $\dot{V}_c$ are consistent with predictions made elsewhere [8].

Fractograms of narrow polystyrene latex standards and the broad PVC latex are superimposed in Fig. 6.

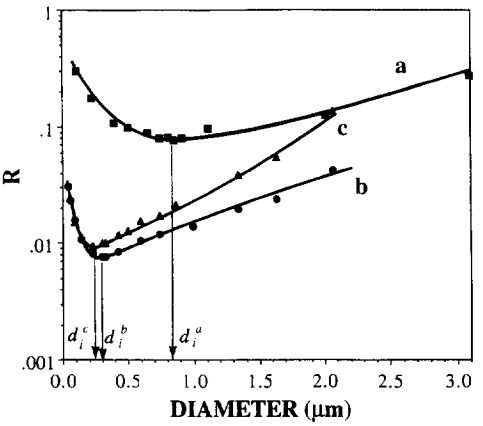

Fig. 5. Plots of R versus d showing that the minimum in R and the corresponding inversion diameter d_i can be shifted substantially using different channels and experimental conditions. (a) $w=179$ μm, $\dot{V}=3.93$ ml/min, and $\dot{V}_c=0.22$ ml/min; (b) $w=85$ μm, $\dot{V}=29.9$ ml/min, and $\dot{V}_c=10.7$ ml/min; (c) $w=75$ μm, $\dot{V}=47.0$ ml/min, and $\dot{V}_c=10.8$ ml/min. Normal mode separation takes place on the left hand side of each d_i and steric-hyperlayer mode on the right side.

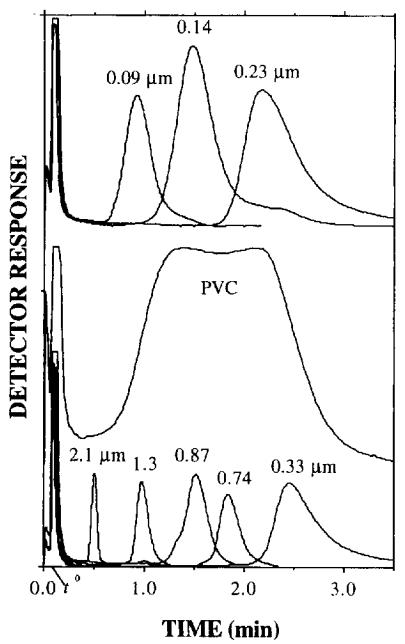

Fig. 6. Fractograms of narrow PS latex standards and polydisperse PVC latex obtained under identical conditions: $w=71$ μm, $\dot{V}=13.4$ ml/min, and $\dot{V}_c=2.95$ ml/min.

These fractograms were obtained in a channel with $w=71$ μm at flow-rates of $\dot{V}=13.4$ ml/min and $\dot{V}_c=2.95$ ml/min. The d_i value, identified as above from the narrow standards, is in the proximity of 0.3 μm. No particles, no matter what their size or composition, should elute at a time beyond that for d_i. The fractograms of Fig. 6, if we ignore the low lying tails, are consistent with this concept, yielding no significant signal beyond 3 min.

5. Conclusion

While the present study demonstrates that high efficiency, high speed, and reduced d_i values can be achieved in unusually thin flow FFF channels, our calculations show that performance still falls short of theoretical expectations. To further improve performance, more work is needed to elucidate and in general find means to circumvent the roles of reversible immobilization, membrane heterogeneity, channel nonuniformity, and other nonidealities in flow FFF separation.

6. Symbols

b	Channel breadth
d	Particle diameter
d_i	Steric inversion diameter
D	Diffusion coefficient
H	Plate height
H_D	Plate height contribution from longitudinal diffusion
$H_{(exp)}$	Experimentally measured plate height corrected for polydispersity
H_n	Plate height contribution from nonequilibrium band broadening
$H_{n(theor)}$	H_n calculated from Eq. (5) using measured retention ratios
$H_{(obs)}$	Experimentally measured plate height
H_p	Plate height contribution from sample polydispersity
ΣH_i	Sum of plate height contributions due to system non-idealities
l	Mean layer thickness (mean distance of particle from accumulation wall)

L	Volume-based channel length
N	Number of plates
R	Retention ratio
S_d	Diameter based selectivity (equal to unity for flow FFF)
t	Unit time
t^0	Channel void time
$\langle v \rangle$	Mean channel flow velocity
$\dot{V}$	Channel flow-rate
$\dot{V}_c$	Cross flow-rate
w	Channel thickness
γ	Dimensionless steric correction factor
λ	Retention parameter (equal to l/w)
σ_d	Standard deviation in the particle diameter

Acknowledgments

This work was supported by NIH Grant No. GM10851-38. We thank P.S. Williams of the Department of Chemistry, University of Utah, for use of his program to calculate various theoretical values.

References

[1] J.C. Giddings, Science, 260 (1993) 1456.
[2] J.C. Giddings, S.K. Ratanathanawongs and M.H. Moon, Kona: Powder and Particle, 9 (1991) 200.
[3] J.C. Giddings and K.D. Caldwell, in B.W. Rossiter and J.F. Hamilton (Editors), Physical Methods of Chemistry, Vol. 3B, Wiley, New York, 1989, Ch. 8, p. 867.
[4] J.C. Giddings, Unified Separation Science, Wiley, New York, 1991, p. 77.
[5] P.S. Williams, T. Koch and J.C. Giddings, Chem. Eng. Comm., 111 (1992) 121.
[6] S.K. Ratanathanawongs and J.C. Giddings, Anal. Chem., 64 (1992) 6.
[7] P.S. Williams, S. Lee and J.C. Giddings, Chem. Eng. Comm., 130 (1994) 143.
[8] J.C. Giddings, Analyst, 118 (1993) 1487.
[9] S.K. Ratanathanawongs and J.C. Giddings, in T. Provder (Editor), Chromatography of Polymers: Characterization by SEC and FFF (ACS Symposium Series, No. 521), American Chemical Society, Washington, DC, 1993, Ch. 2, p. 13.
[10] S. Lee and J.C. Giddings, Anal. Chem., 60 (1988) 2328.
[11] K.-G. Wahlund, H.S. Winegarner, K.D. Caldwell and J.C. Giddings, Anal. Chem., 58 (1986) 573.
[12] J.C. Giddings, M.N. Myers, K.D. Caldwell, J.W. Pav, J. Chromatogr., 185 (1979) 261.
[13] K.D. Caldwell, T.T. Nguyen, M.N. Myers, J.C. Giddings, Sep. Sci. Technol., 14 (1979) 935.
[14] A.J. Goldman, R.G. Cox, H. Brenner, Chem. Eng. Sci., 22 (1967) 653.
[15] J.C. Giddings and F.-S. Yang, J. Colloid Interface Sci., 105 (1985) 55.
[16] P.S. Williams and J.C. Giddings, Anal. Chem., 66 (1994) 4215.
[17] J.C. Giddings, F.J. Yang and M.N. Myers, Anal. Chem., 48 (1976) 1126.
[18] A.M. Botana, S.K. Ratanathanawongs and J.C. Giddings, J. Microcol. Sep., 7 (1995) 395.
[19] S.K. Ratanathanawongs, I. Lee and J.C. Giddings, in T. Provder (Editor), Particle Size Distribution II: Assessment and Characterization (ACS Symposium Series, No. 472), American Chemical Society, Washington, DC, 1991, Ch. 15, p. 229.
[20] J.C. Giddings, P.S. Williams and M.A. Benincasa, J. Chromatogr., 627 (1992) 23.
[21] J.C. Giddings, Anal. Chem., 62 (1990) 2306.
[22] J.M. Davis, Anal. Chim. Acta., 246 (1991) 161.
[23] M.-K. Liu, P. Li and J.C. Giddings, Protein Science, 2 (1993) 1520.
[24] A. Litzén and K.-G. Wahlund, J. Chromatogr., 548 (1991) 393.